JOURNAL OF GEOPHYSICAL RESEARCH, VOL. 113, A09215, doi:10.1029/2008JA013340, 2008

Response of the expanding/contracting polar cap to weak and strong solar wind driving: Implications for substorm onset

S. E. Milan,[1] P. D. Boakes,[1] and B. Hubert[2]

Received 21 April 2008; revised 11 June 2008; accepted 9 July 2008; published 11 September 2008.

[1] We quantify the amount of open magnetic flux in the magnetosphere from observations of the auroral polar cap on a near-continuous basis for a period of 18 days, 20 August to 6 September 2005. This interval encompasses periods of weak, moderate, and strong solar wind driving, including two geomagnetic storms. We identify 49 substorms during the interval and determine the response of the polar cap to growth and expansion phases of the substorms. We find that the frequency of substorms and the flux closed by substorms both increase during enhanced solar wind driving, each approximately as the square root of the dayside reconnection rate. In addition, the average size of the polar cap increases during intervals when there is strong driving and especially when the SYM-H index indicates that the ring current is enhanced. We suggest that this occurs for two reasons: because there is a delay between substorm onset and the closure of open magnetic flux in the magnetotail (while closed flux is pinched off), during which dayside reconnection can lead to further growth in the size of the polar cap, and also because the magnetotail is more stable to reconnection when the ring current is enhanced.

Citation: Milan, S. E., P. D. Boakes, and B. Hubert (2008), Response of the expanding/contracting polar cap to weak and strong solar wind driving: Implications for substorm onset, *J. Geophys. Res.*, *113*, A09215, doi:10.1029/2008JA013340.

1. Introduction

[2] Dynamic activity in the terrestrial magnetosphere is driven by momentum and energy transfer from the solar wind, mediated by magnetic reconnection between the interplanetary magnetic field (IMF) carried by the outflowing plasma and the Earth's magnetic field at the dayside magnetopause [*Dungey*, 1961, 1963]. Reconnection occurs where there is a large shear angle between the IMF and the terrestrial field. When the IMF is directed southward, this occurs near the equatorial plane of the magnetopause, the reconnecting terrestrial magnetic field lines becoming open, that is, connecting into the solar wind. These open field lines are stretched into a long magnetotail by the flow of the solar wind, and are subsequently closed again by reconnection in the tail neutral sheet. The cycle of opening and closing field lines, the Dungey cycle, leads to the circulation and structuring of plasma within the magnetosphere; the projection of this circulation into the ionosphere results in the polar ionospheric convection pattern. For northward-directed IMF, magnetopause reconnection occurs at high latitudes, tailward of the cusp openings, with already open lobe field lines. As this process does not produce new open flux, the Dungey cycle is not strongly driven for this case.

[3] The amount of open flux in the magnetosphere, F_{PC}, can be estimated from the size of the ionospheric polar caps, the dim regions enclosed within the auroral ovals [*Milan et al.*, 2003]. As dayside and magnetotail reconnection occur independently of each other the amount of open flux varies with time, and the polar caps expand and contract as the open flux waxes and wanes. *Milan et al.* [2007] estimated that F_{PC} varies between approximately 0.2 and 1 GWb, that is 3 and 12% of the flux associated with each hemisphere of the terrestrial dipole. *Siscoe and Huang* [1985] and *Cowley and Lockwood* [1992] demonstrated how this expanding/contracting polar cap (ECPC) paradigm could naturally explain the ionospheric convection pattern observed for southward IMF. *Lockwood and Cowley* [1992] further speculated that the closure of open flux on the nightside was mainly associated with substorm activity, making substorms an integral component of the Dungey cycle and the excitation of ionospheric convection. Recently, by examining 73 hours of measurements of F_{PC}, spread over 9 intervals, *Milan et al.* [2007] confirmed this picture and quantified the open flux throughput of the system. They demonstrated that nightside reconnection events typically close 0.3 GWb of open flux, occur preferentially when $F_{PC} > 0.5$ GWb and increase in probability as F_{PC} grows toward 1 GWb. *Kamide et al.* [1977] also proposed that the occurrence of substorms increases as the amount of open flux in the tail grows. *Milan et al.* [2007] also showed that approximately 50% of the events could be associated with a trigger in the solar wind (a sudden change of the north-south orientation of the IMF or a step in solar wind ram pressure),

[1]Department of Physics and Astronomy, University of Leicester, Leicester, UK.
[2]Laboratory of Planetary and Atmospheric Physics, University of Liège, Liege, Belgium.

0148-0227/08/2008JA013340$09.00

while the rest occurred spontaneously, almost exclusively during periods of ongoing southward IMF.

[4] This raises questions as to the mechanism by which substorm onset is initiated. It is manifestly true that external triggers can cause onset, for instance solar wind shocks have been implicated by several studies [e.g., *Boudouridis et al.*, 2003; *Milan et al.*, 2004; *Hubert et al.*, 2006b]. Increased pressure on the tail can compress the plasma sheet and lead to conditions favorable to onset. This also works for spontaneous onset: as suggested by *Slavin et al.* [2002] as the open flux content of the tail increases the magnetopause flares outward, increasing the normal stress exerted by the solar wind, again raising the internal pressure. The exact conditions in the tail necessary for substorm onset, and the triggering of magnetic reconnection to reduce the open flux content of the magnetosphere, have been under considerable debate for many years [e.g., *Cheng*, 2004, and references therein]. Previous authors have examined the loading/unloading or inflation/deflation signatures observed in the tail during the substorm cycle [e.g., *Nakai and Kamide*, 2003; *Tanskanen et al.*, 2005]. In this study we investigate, in addition, the variation in open flux in the magnetosphere during this cycle.

[5] We examine near-continuous measurements of F_{PC} during the 18 day period 20 August to 6 September 2005, which includes intervals of fast and slow solar wind speed, high and low solar wind ram pressure, and a wide range of IMF orientation and strength. The magnetospheric response to these inputs varies between intervals of almost complete quiescence to a −180 nT SYM-H geomagnetic storm.

2. Observations

[6] We study the solar wind conditions from 20 August to 6 September 2005, monitored by the ACE spacecraft [*McComas et al.*, 1998; *Smith et al.*, 1998; *Stone et al.*, 1998] located at L1, and the associated magnetospheric response determined from Southern Hemisphere auroral emissions observed by the Wideband Imaging Camera of the Far-Ultraviolet Imager (FUV/WIC) onboard the IMAGE spacecraft [*Mende et al.*, 2000a, 2000b]. Simultaneous observations of the magnetotail magnetic field are provided by the Fluxgate Magnetometer (FGM) on the Cluster spacecraft [*Balogh et al.*, 1997, 2001]. Ground magnetometers provide the auroral indices AU and AL [*Davis and Sugiura*, 1966] and SYM-H, similar to the D_{st} index.

[7] The solar wind and IMF conditions during the 18 day interval are summarized in Figures 1a–1e. Figure 1a presents the solar wind speed, V_X, and Figure 1b presents the solar wind ram or dynamic pressure P_{dyn}. The GSM Y and Z components of the interplanetary magnetic field, IMF B_Y and B_Z, are presented in Figures 1c and 1d. It is also useful to estimate the dayside reconnection voltage Φ_D from the solar wind conditions, for which we use the expression

$$\Phi_D = L_{eff} V_X \sqrt{B_Y^2 + B_Z^2} \sin^2 \frac{1}{2}\theta$$

which is the *Kan and Lee* [1979] reconnection electric field multiplied by a characteristic scale length $L_{eff} = 2.75\ R_E$ (see Appendix A for more details). Φ_D is shown in Figure 1e.

[8] Examination of the solar wind speed shows that during the 18 day period there are two intervals of elevated outflow, roughly 22–26 August and 1–5 September, peaking between 700 and 800 km s^{-1}. In each case, the speed increases in steps and the interaction between faster solar wind streams catching up with preceding slower streams results in solar wind density peaks and IMF flux pile-up, especially on 21, 24, and 31 August and 2 September. The background ram pressure and IMF field strength are 2 nPa and 5 nT. The enhancements in most cases are approximately 10 nPa and 20 nT, with the exception of the disturbance of 24 August when peak values reach 30 nPa and 60 nT. The predicted dayside reconnection voltage reaches 100–150 kV on 31 August and 2 September, and exceeds 300 kV on 24 August. During the rest of the interval there are periods when the reconnection voltage remains somewhat elevated, varying between 30 and 80 kV (e.g., 3–7 September), and when it is very low, below 30 kV, for prolonged periods (e.g., 26–30 August).

[9] Ground magnetic signatures of the magnetospheric response to the solar wind conditions are shown in Figure 1h (AU, AL) and Figure 1i (SYM-H). A clear response to the solar wind disturbances is seen in SYM-H, which displays the characteristic initial, main, and recovery phase signatures of geomagnetic storms commencing the 24 and 31 August, with minima of −180 and −110 nT, respectively. The response in AL and AU during the two storms is also clear, with enhanced substorm activity during each period. In addition, close examination of the response of AU and AL to changes in the predicted dayside reconnection rate (Figure 1e) shows a very close association.

[10] The remaining two panels of Figure 1 show the nightside auroral brightness (Figure 1f) and open flux content of the magnetosphere F_{PC} (Figure 1g) determined from the auroral observations made by IMAGE FUV/WIC. These will be examined in more detail below. For the present, we note that there is again a close association between elevated dayside reconnection rates and elevated brightness and open flux content. In what follows we will mainly focus on the period from 28 August onward (marked by the vertical dotted line), as prior to this inaccuracies in the pointing information of IMAGE result in increased uncertainties in our determination of F_{PC}.

[11] We now examine the auroral observations made by IMAGE FUV/WIC and measurements of the magnetotail field made by Cluster FGM. We do this in Figures 2 and 3 for the two intervals indicated at the top of Figure 1. Each of these intervals corresponds to one orbit of Cluster; during each the orbital plane was contained almost in the X–Z plane with apogee in the magnetotail. These two orbits allow us to investigate the difference between strongly and more moderately driven conditions. Figures 2g and 2h and Figures 3g and 3h show the total field strength, B_T, and the Z component of the field, B_Z, measured by Cluster 1 (C1). C1 is close to the Earth where B_T is high at the start and end of each figure, and passes through the neutral sheet where B_T goes close to 0 nT. Overlaid as thin lines are T96 [*Tsyganenko and Stern*, 1996] model fits to these parameters. The concurrent ACE solar wind and IMF measurements of P_{dyn} and IMF B_Y and B_Z, as well as D_{st}, have been used as input to the model; where P_{dyn} was not available (Figure 2) a value of 2 nPa was used. The model prediction of both B_T and B_Z is very good in Figure 3 and not as good in Figure 2.

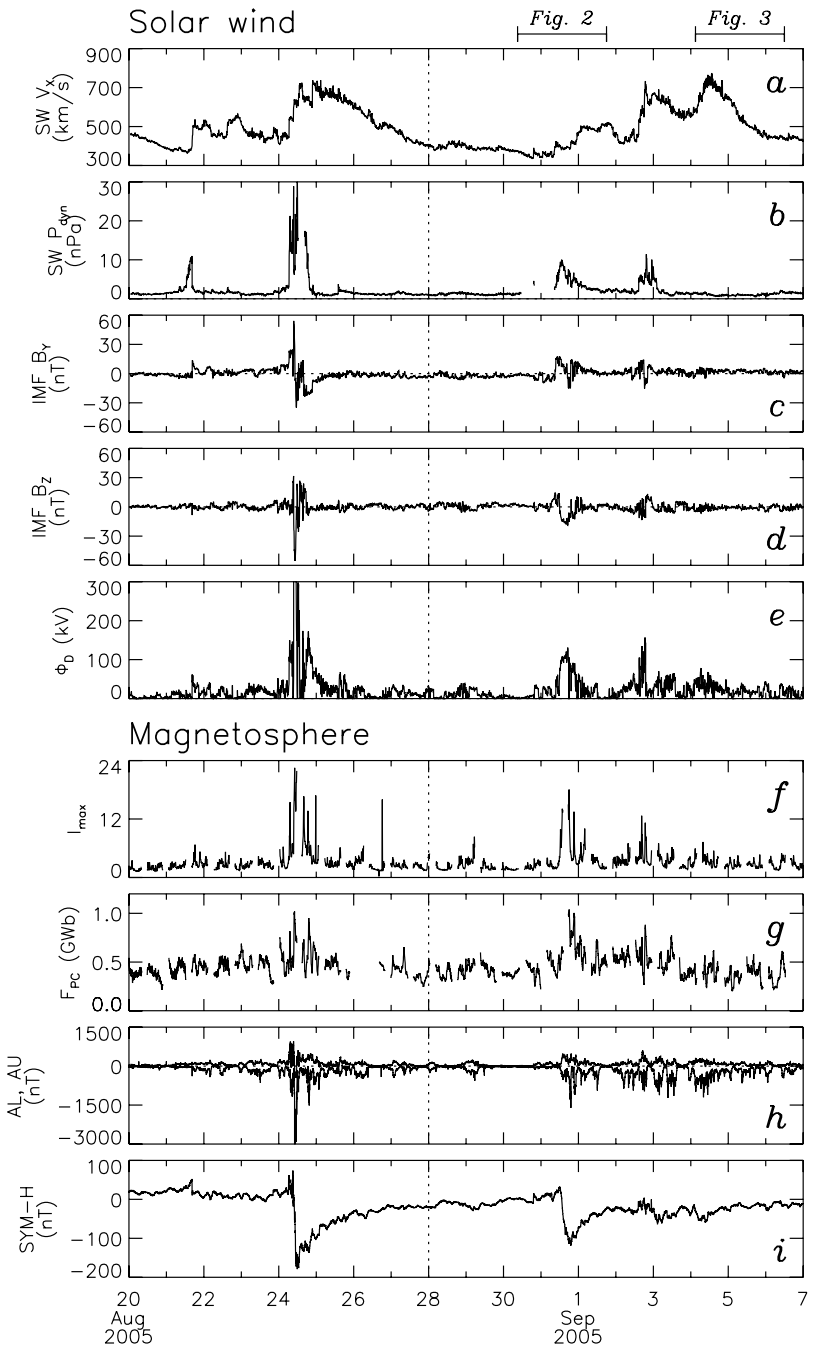

Figure 1. Auroral, magnetotail, and solar wind observations for the 18 day period 20 August to 6 September 2005. (a) The solar wind speed, (b) the solar wind dynamic pressure P_{dyn}, and (c and d) the B_Y and B_Z GSM components of the IMF, all as measured by ACE. (e) Predicted dayside reconnection rate, Φ_D, derived from IMF B_Y, B_Z and solar wind V_X. (f) The maximum auroral intensity on the nightside, I_{max}, as measured by the IMAGE FUV/WIC camera (arbitrary units). (g) The open flux content of the magnetosphere, F_{PC}, derived from the auroral observations. (h) AU and AL geomagnetic auroral indices. (e) SYM-H index.

[12] Away from the planet and the neutral sheet crossings C1 is located in the magnetotail lobes. The field strength in the lobes B_L can be used to give an indication of the magnetic pressure in the tail, $P_{mag} = B_L^2/2\mu_0$. Within the plasma sheet, which is expected to be in stress balance with the lobes, plasma pressure contributes to the overall balance and the magnetic pressure dips. The tail itself is in stress balance with the magnetosheath plasma outside, so the internal pressure is related to the solar wind ram pressure. Indeed, comparing the two orbits, enhanced solar wind ram pressure (Figure 2k) is matched by higher values of B_T. T96 also predicts higher B_T in Figure 2, but not sufficiently to match the observations. As we will discuss below, this is

due to changes in the open flux content of the magnetosphere, which is not parameterized in T96.

[13] Figures 2a and 2b and Figures 3a and 3b show noon-midnight and dawn-dusk keograms of the Southern Hemisphere auroral emission observed by IMAGE FUV/WIC. For each available WIC image the auroral intensity along either noon-midnight or dawn-dusk meridian is plotted vertically, with time running horizontally. In this way it is possible to see the time variation in the size of the polar cap, the dim region inside the auroral oval, that region of the ionosphere mapping magnetically into the magnetotail lobes. Dayglow is evident in the noon sector (tops of Figures 2a and 3a), encroaching to higher or lower magnetic latitudes as the Earth's southern dipole axis rocks toward and away from the Sun. Gaps in the observations are due to the orbit of the IMAGE spacecraft, appearing when it is at perigee over the Northern Hemisphere; both Figures 2 and 3 correspond to 4 orbits of IMAGE. Significant auroral brightenings, indicating the occurrence of substorms, are apparent in the midnight sector auroral oval, usually displaying the characteristic poleward progression of the substorm auroral bulge. Larger events are also visible along the dawn and dusk meridians. To aid identification of substorms, Figures 2c and 3c show the maximum auroral brightness observed in the nightside auroral oval, I_{max} (in arbitrary units). Using this, and other signatures described below, we identified 49 substorms during the 10 day period of interest, and these have been indicated by thin vertical lines. From each available auroral image the size of the polar cap was measured using the techniques described by *Milan et al.* [2003], from which the open magnetic flux F_{PC} was calculated; this is presented in Figures 2d and 3d.

[14] Concentrating on the interval 12 UT, 31 August, to 00 UT, 1 September, in Figure 2, the behavior of the magnetosphere during substorms is clear. Usually, preceding each event the polar cap expands and F_{PC} increases (Figure 2d) owing to ongoing dayside reconnection $\Phi_D > 0$ kV (Figure 2j): the substorm growth phase. By Faraday's Law, the rate of increase of F_{PC} should be equal to Φ_D, assuming that no nightside reconnection is ongoing at the time. Eventually, expansion phase onset is triggered, nightside reconnection commences, the nightside auroral luminosity suddenly increases and the polar cap contracts (F_{PC} decreases). Onset is usually accompanied by a negative excursion in the AL index (Figure 2e) owing to the formation of the westward substorm auroral electrojet. In the lobes of the magnetotail, during the growth phase the field strength B_T increases (Figure 2g). This occurs owing to the increase in F_{PC}, which causes the magnetotail to flare outward such that the stress exerted by the magnetosheath flow on the magnetopause grows. That is, as the open flux increases the tail simultaneously expands outward and the field inside is compressed. At substorm onset, as open flux is closed, the pressure in the tail is alleviated and B_T decreases (Figure 2g). There is a simultaneous positive excursion of the B_Z component of the field (Figure 2h) indicating that the tail relaxes to a more dipolar configura-

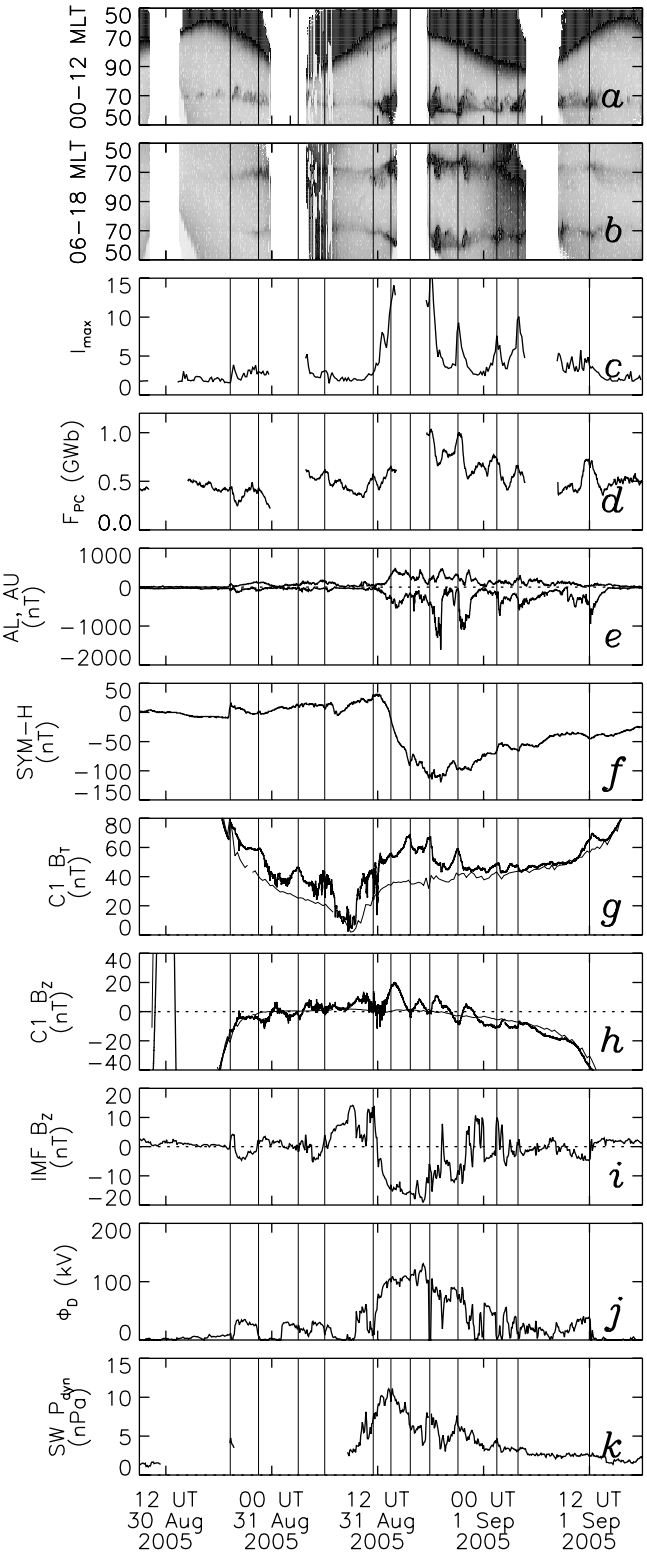

Figure 2. Auroral, magnetotail, and solar wind observations from the interval corresponding to an orbit of Cluster occurring during strong solar wind driving conditions. Keograms of auroral activity derived from IMAGE FUV/WIC observations, along (a) the noon-midnight and (b) the dawn-dusk meridians. (c) I_{max}, (d) F_{PC}, (e) AU and AL, (f) SYM-H, (g) total and (h) Z-component magnetic field B_T and B_Z measured by Cluster C1 FGM (including T96 predictions), (i) IMF B_Z, (j) Φ_D, and (k) P_{dyn}. Vertical lines indicate the times of substorm onsets.

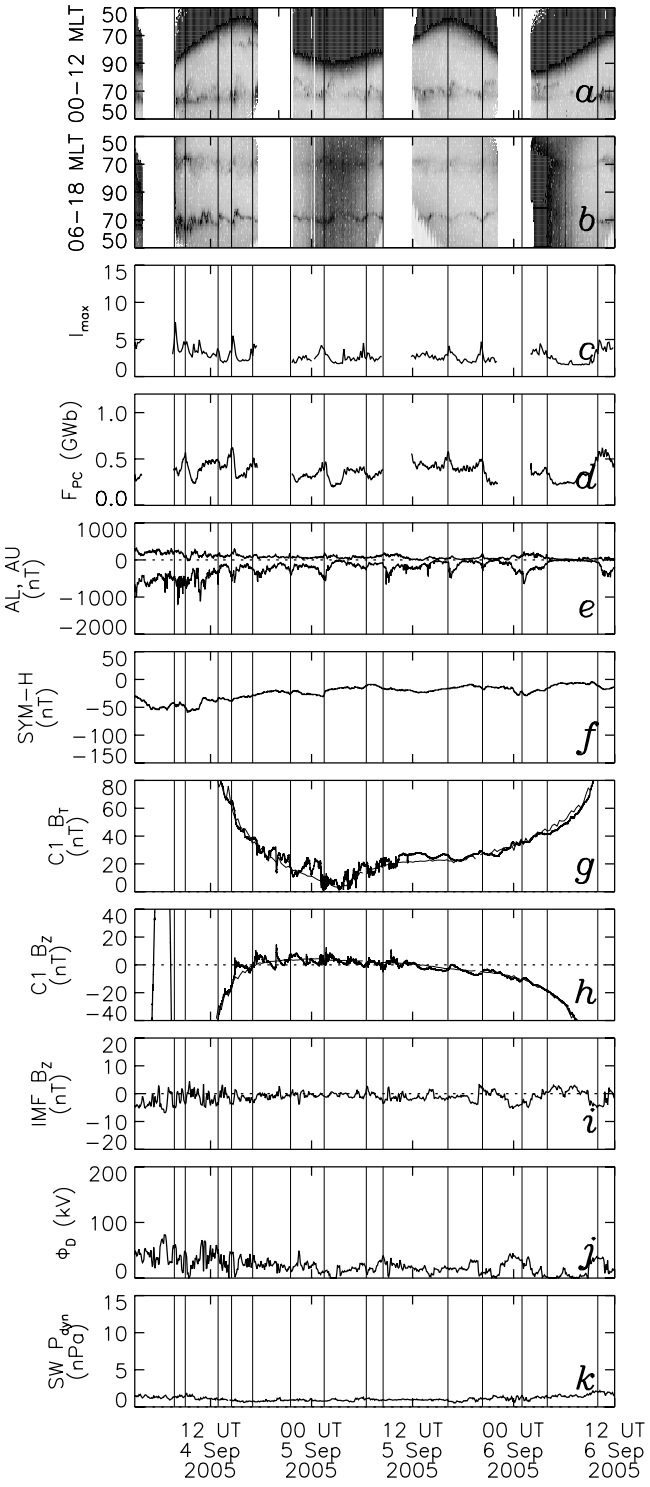

Figure 3. Similar to Figure 2, showing the an orbit of Cluster occurring during moderate solar wind driving.

tion as flux closure progresses. Expansion phase signatures, enhanced auroral brightness, polar cap contraction, AL bay, decreasing tail pressure, and dipolarization, continue in general for 1 to 2 hours. Thereafter, if $\Phi_D > 0$ kV the cycle repeats. These tail dynamics are consistent with those described by, e.g., *Nakai and Kamide* [2003] and *Tanskanen et al.* [2005]; here we confirm for the first time that these dynamics are associated with changes in the open flux content of the magnetosphere, F_{PC}.

[15] These substorm signatures are observed throughout the interval investigated. However, they are much more pronounced when the solar wind driving is strong, i.e., Φ_D is high. For instance, in Figure 3 the auroral luminosities are much lower than in Figure 2, the negative excursions in AL are less extreme, and the excursions in the tail field associated with substorm growth and dipolarization are smaller. Substorms also occur less frequently and tend to be isolated events rather than a continuous train. It is also noticeable that substorms during this period occur for a smaller polar cap, $F_{PC} \approx 0.5$ GWb (Figure 3d), whereas F_{PC} rises as high as 1 GWb during more driven periods (Figure 2d).

3. Discussion

[16] We have quantified the expanding/contracting nature of the polar cap, that is the variation in F_{PC}, for an 18 day interval encompassing low, moderate and high solar wind driving. F_{PC} is found to vary between approximately 0.2 and 1 GWb. Typically, F_{PC} is less than 0.6 GWb, but increases significantly above this during periods of intense dayside coupling. Owing to increased uncertainties in our estimates of F_{PC} prior to the 28 August, we concentrate on the last 10 days of observations. The occurrence distribution of F_{PC} for this period is presented in Figure 4, from which we calculate a mean value of F_{PC} of 0.42 GWb. Overlaid is the open flux distribution determined by *Milan et al.* [2007] from a smaller sample of data; a Kolmogorov-Smirnov analysis indicates that the two distributions are similar at a confidence level of greater than 0.999.

[17] We now examine the occurrence of substorms and the amount of open flux closed by substorms during different levels of dayside coupling in Figure 5. Figure 5a reproduces the variation of F_{PC} for the 10 days of interest; Φ_D for this period is shown in Figure 5d. Figure 5b presents

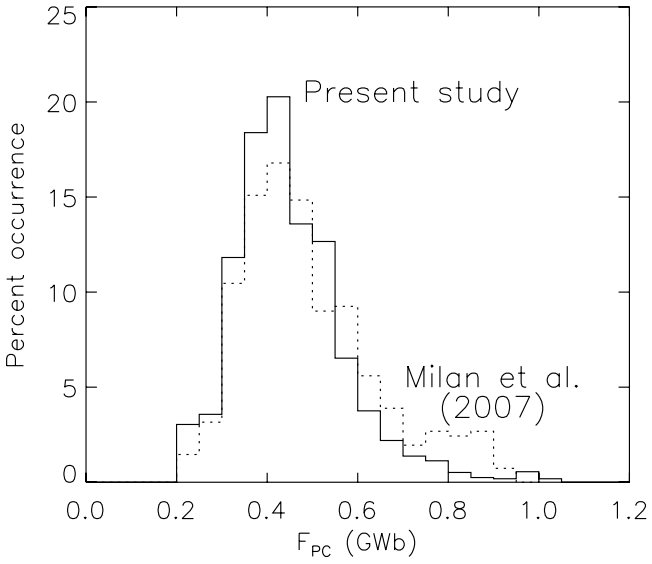

Figure 4. The occurrence distribution of F_{PC} for the 10 day period 28 August to 6 September. Superimposed is the occurrence distribution found by *Milan et al.* [2007].

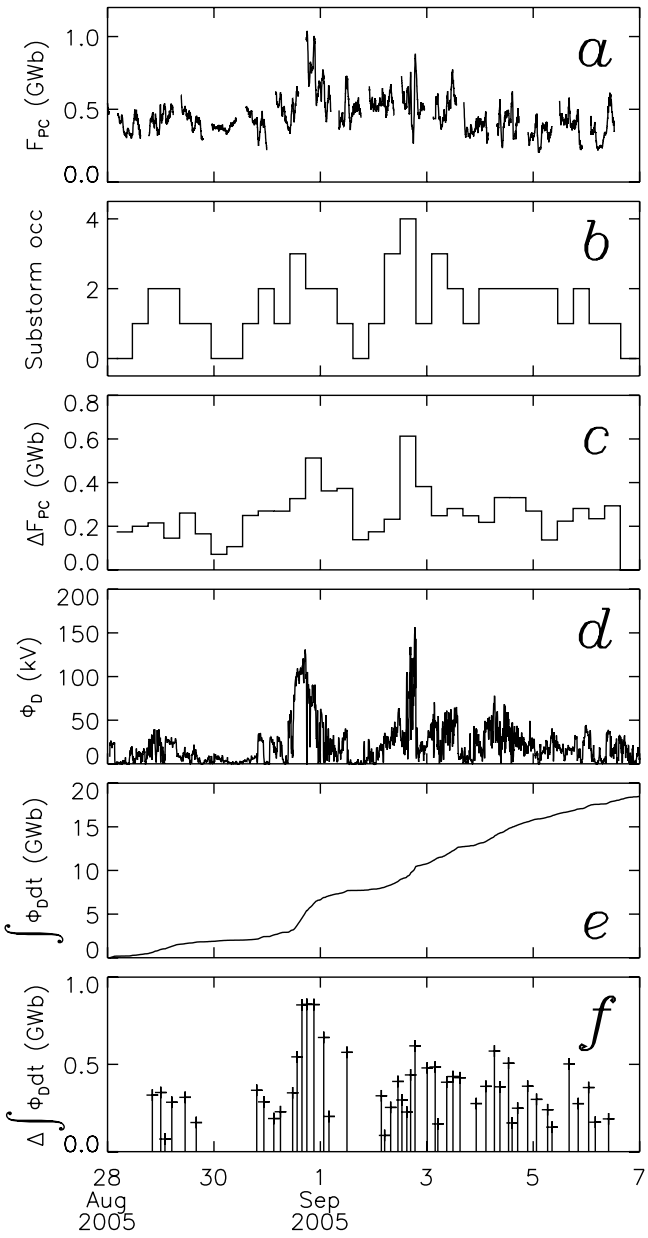

Figure 5. (a) F_{PC} for the 10 day interval. (b) Substorm occurrence in 7.1-hour bins. (c) The range index ΔF_{PC}, indicating the variation in F_{PC}, in 7.1-hour bins. (d) The predicted Φ_D. (e) Integrated Φ_D for the 10 day interval. (f) Integrated Φ_D between each substorm onset.

a count of the number of substorms detected during this period in 7.1-hour bins; 7.1 hours is chosen to correspond to half an IMAGE orbit, so each bin contains exactly half an IMAGE perigee pass data gap. From Figure 5 it is clear that substorm occurrence peaks when the Φ_D is greatest. This is due to the rapid accumulation of open flux at the magnetopause during such periods, and so the more flux that must be released in the tail. In Figure 5c we introduce the range index ΔF_{PC} which indicates the difference between the maximum and minimum values of F_{PC} in each of the 7.1-hour bins; from this we wish to gauge by how much F_{PC} fluctuates during substorms under different driving conditions. Again, it is clear that ΔF_{PC} maximizes when Φ_D is large. Figure 5e shows the integral of Φ_D with time, $\int \Phi_D dt$. This suggests that the magnetosphere captured approximately 19 GWb of solar wind magnetic flux during the period considered. This accumulating flux is released episodically by the occurrence of substorms. Figure 5f shows, for each of the 49 substorms identified earlier, the amount of flux accumulated since the previous substorm onset, which we might write as $\Delta \int \Phi_D dt$. This might also be considered to be the amount of flux that needs to be released by each substorm. Encouragingly, this matches approximately the variation in ΔF_{PC}.

[18] There are interesting correspondences between Figures 5a, 5b, 5c, 5d, and 5f. The open flux in the polar cap undergoes an expanding/contracting behavior in response to dayside flux accumulation and release by substorms. However, the maximum F_{PC} attained prior to substorm onset is greater when Φ_D is large. F_{PC} decreases during substorms, but if the driving is strong it remains relatively elevated even at its minima, especially true on 31 August. In other words, tail reconnection associated with each substorm appears to cease while the tail is still in a stressed state if Φ_D is large (or, as is discussed below, if SYM-H indicates the presence of a significant ring current). In addition, the flux accumulated prior to each substorm (Figure 5f) is greatest when the driving is strong. This also corresponds to times when the variation in F_{PC}, as quantified by ΔF_{PC}, is large (Figure 5c), suggesting that the release of flux during substorms is indeed greatest during such periods.

[19] The overall rate of closure of open flux by substorms depends on the frequency with which substorms occur and the amount of flux released by each. We can ask: when the rate of open flux accumulation at the dayside increases, is the required release of open flux on the nightside provided by an increased frequency of substorms or larger substorms? This question is addressed in Figure 6. We have divided the time interval into 7.1-hour bins (as per Figure 5), and determined the time-averaged dayside reconnection rate $\langle \Phi_D \rangle$ within each bin. Figure 6a then shows the average frequency of occurrence of substorms in each bin f_S (s^{-1}), that is the substorm occurrence (Figure 5b) divided by the bin width (25560 s), as a function of $\langle \Phi_D \rangle$. Figure 6b shows the range index ΔF_{PC} (Figure 5c), which we take to be a crude measure of the amount of flux released in each substorm, as a function of $\langle \Phi_D \rangle$. Finally, Figure 6c presents $f_S \times \Delta F_{PC}$, an estimate of the average rate of flux closure in each bin, $\langle \Phi_N \rangle$. It is clear that as the flux accumulation rate increases, this flux closure rate increases also, as expected. In addition, both the closure of flux during individual substorms and the occurrence of substorms increase during elevated solar wind driving.

[20] To understand these results we first write that over a sufficiently long time interval the time-averaged release of flux must be equal to the time-averaged rate of flux accumulation:

$$\langle \Phi_N \rangle = \langle \Phi_D \rangle.$$

If we then say that the rate of closure of flux is dependent on the substorm frequency f_S and the flux closed in each

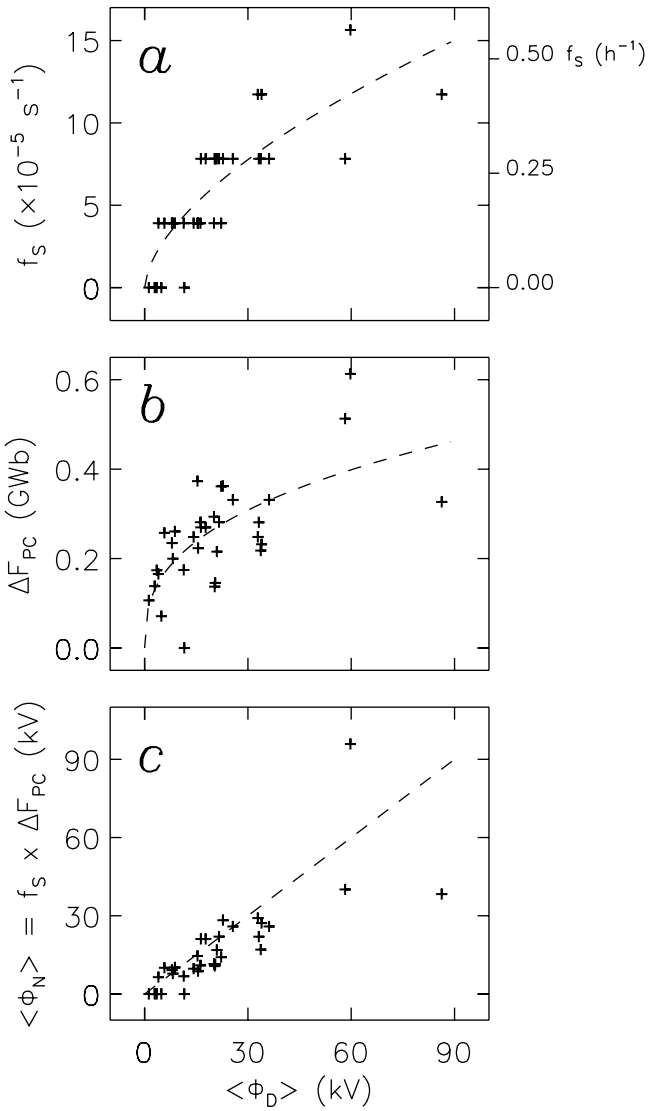

Figure 6. (a) The substorm frequency in 7.1-hour bins (see also Figure 5b) as a function of the average dayside reconnection rate $\langle \Phi_D \rangle$ in each bin. (b) The range index ΔF_{PC} in each 7.1-hour bin (see also Figure 5c) as a function of $\langle \Phi_D \rangle$. (c) A measure of the average nightside reconnection rate $\langle \Phi_N \rangle$ in each 7.1-hour bin as a function of $\langle \Phi_D \rangle$.

substorm, both of which are controlled by the ongoing dayside flux accumulation rate, we have:

$$\langle \Phi_N \rangle = f_S(\langle \Phi_D \rangle) \times \Delta F_{PC}(\langle \Phi_D \rangle).$$

Finally, we assume simple dependencies of f_S and ΔF_{PC} on $\langle \Phi_D \rangle$, which require that $f_S = \Delta F_{PC} = 0$ when $\langle \Phi_D \rangle = 0$:

$$f_S(\langle \Phi_D \rangle) = A\langle \Phi_D \rangle^{\alpha},$$

$$\Delta F_{PC}(\langle \Phi_D \rangle) = B\langle \Phi_D \rangle^{\beta},$$

where A, B, α and β are to be determined. Taken together, these relations imply that:

$$\langle \Phi_N \rangle = A\langle \Phi_D \rangle^{\alpha} \times B\langle \Phi_D \rangle^{\beta} = AB\langle \Phi_D \rangle^{\alpha+\beta} = \langle \Phi_D \rangle$$

or, in other words, $\alpha + \beta = 1$ and $AB = 1$. If the increased rate of flux release was achieved by more frequent substorms each of the same size then $\alpha = 1$, $\beta = 0$; conversely, if the size of the substorms increased but their frequency remained constant then $\alpha = 0$, $\beta = 1$. However, we observe an increase in both f_S and ΔF_{PC}. We determine A, B, α and β from the observations in Figure 6 by a least squares technique and find

$$f_S(\mathrm{s}^{-1}) = 1.7 \times 10^{-7}\langle \Phi_D \rangle^{0.60},$$

$$\Delta F_{PC}(\mathrm{Wb}) = 6.8 \times 10^{6}\langle \Phi_D \rangle^{0.37}$$

where $\langle \Phi_D \rangle$ is expressed in V; these fits are indicated in Figures 6a and 6b by dashed curves. Despite there being considerable scatter in the points and the uncertainties in the fitting are quite large, especially in the values of A and B, we find that these fits closely satisfy our expectation that $\alpha + \beta = 1$ and $AB = 1$. In other words, the frequency of substorms and the flux closed in each both increase as approximately the square root of the dayside driving rate.

[21] Not only do the substorm occurrence rate and the overall flux closure rate increase during periods of strong solar wind driving, but also the polar cap as a whole becomes enlarged (compare Figures 5a and 5d). That is, F_{PC} is larger at substorm onset during such periods, and although it contracts during the course of each substorm it remains larger than during more quiescent times. For instance, on 31 August (Figure 2) F_{PC} remains elevated above 0.5 GWb during the course of several substorms, whereas more typically it falls to values below 0.4 GWb. We note that this enlarged oval occurs during a period when SYM-H indicates the presence of an intensified ring current (Figure 1). There are two possible interpretations of these findings:

[22] 1. The magnetotail is more stable to reconnection when the driving is strong and/or the ring current is enhanced (see below). This latter has also been suggested by *Nakai and Kamide* [2003].

[23] 2. Substorm onset is set into motion when a certain threshold of accumulated flux is exceeded in the tail, but there is a delay before flux closure becomes efficient and in the meantime the polar cap has expanded owing to ongoing dayside reconnection.

[24] That the latter mechanism does indeed occur is demonstrated in Figure 7. Figures 7a–7d show a sequence of four auroral images, the first prior to substorm onset, the last three during the expansion phase. Each panel is centered on the geomagnetic pole, with magnetic noon to the top and dawn to the right. The dark region at the top of each panel is dayglow. Figures 7e and 7f then show keograms of the midnight and dawn-dusk sectors, the times of the four images indicated at the top of Figure 7e. Figures 7g, 7h, 7i, 7j, and 7k present the nightside auroral brightness, F_{PC}, AL and AU, the B_T and B_Z magnetic field components measured at Cluster, and the dayside reconnection rate Φ_D, respectively. The first auroral image shows that the auroral oval has a well-defined lower-latitude edge and is dimmer at higher latitudes. The location of the open/closed field line boundary (OCB) has been determined as the poleward edge of the dim luminosity and is indicated as a dark line in Figures 7a–7f. Expansion phase onset is seen in Figure 7b

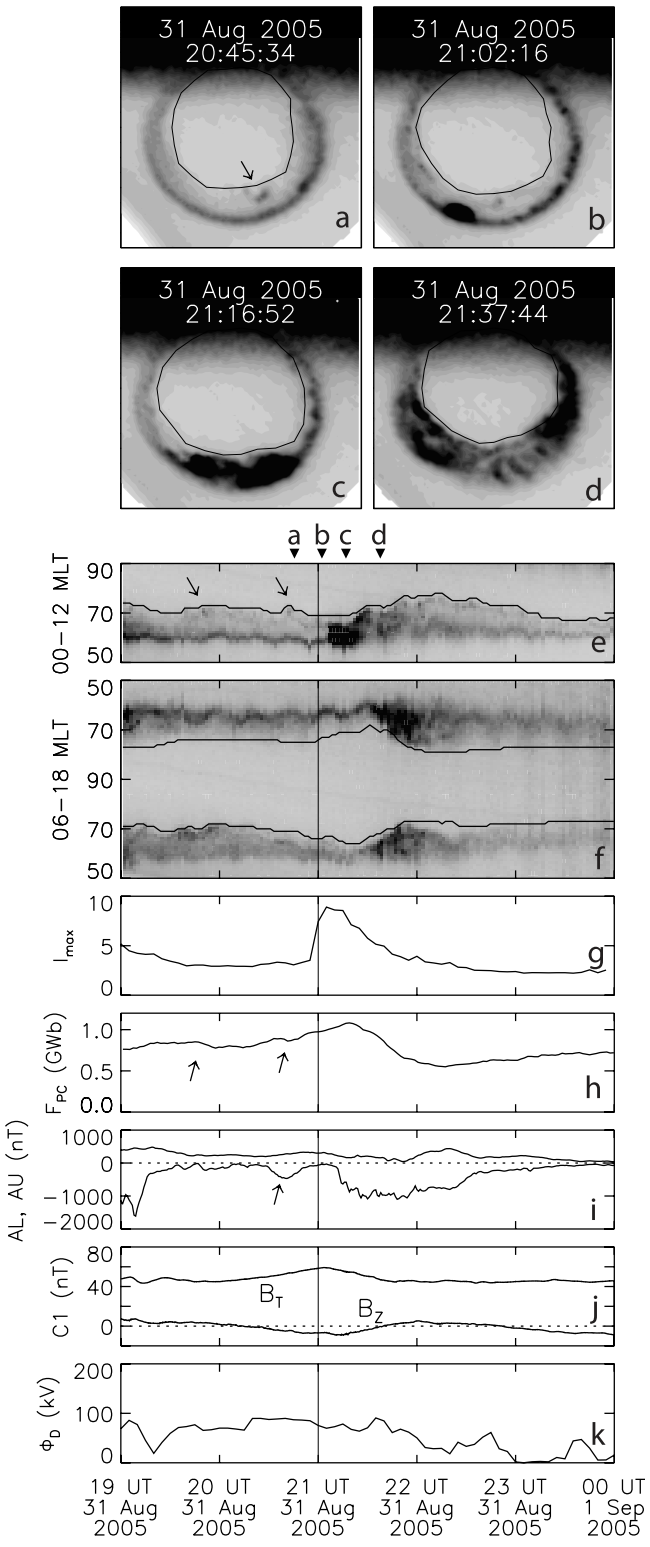

Figure 7. (a–d) Images of the auroral development of a substorm, in a magnetic latitude/MLT frame, with noon to the top of each panel. The thin line indicates the estimated location of the open/closed field line boundary (OCB). Keograms along (e) the noon-midnight and (f) the dawn-dusk meridians for a 5-hour period encompassing the substorm growth, expansion, and recovery phases. Lines indicate the estimated locations of the OCB. (g) I_{max}, (h) F_{PC}, (i) AL and AU, (j) Cluster B_T and B_Z, and (k) Φ_D.

as a brightening of the equatorward edge of the oval in the premidnight sector (seen as a sharp increase in auroral brightness in Figure 7g, also indicated by a vertical line in Figures 7e–7k). Although the breakup aurora spread poleward, dawnward and duskward in Figure 7c, they remain confined to a region of preexisting closed field lines until shortly before Figure 7d. This indicates that reconnection starts in a localized region near the inner edge of the plasma sheet and starts to pinch off closed magnetic field lines; subsequently, reconnection spreads dawnward and duskward. However, the pinch-off is not complete, that is the reconnection does not progress onto open lobe field lines, until 10–15 min after expansion phase onset. Open flux continues to be opened on the dayside at a rate of nearly 100 kV during these 15 min (Figure 7k) leading to a further expansion of the polar cap by at least 0.1 GWb (Figure 7h), and seen most clearly as continued equatorward motion of the OCB along the dawn and dusk meridians (Figure 7f).

[25] B_T measured at Cluster (Figure 7j) begins to decrease within 4 min of substorm onset, indicating that the pressure in the near-tail decreases as closed flux is pinched off, and the start of the dipolarization is seen in B_Z within 12 min. It is interesting to note that the AL signature of the substorm (Figure 7i) is delayed by up to 10 min after onset; this may be due to the spacing between the magnetometer stations from which the auroral indices are derived.

[26] One last point is of interest. Prior to substorm onset, transient brightenings of localized regions of the high-latitude portion of the auroral oval are seen. One is indicated by an arrow in Figure 7a, and this and a previous event are indicated by arrows in Figure 7e. These occur on closed field lines, but presumably map to a considerable distance down-tail, maybe to near the distant X-line. They appear to be associated with very modest contractions of the polar cap (Figure 7h), each less than 0.05 GWb, though the second event is observed in AL (Figure 7i). These signatures may indicate that the stressed magnetotail (F_{PC} is close to 1 GWb at this time) tries to initiate reconnection at a distant X-line, but efficient closure of flux cannot take place until a near-Earth X-line is formed. This behavior is similar to pseudo-breakups, which are known to close magnetic flux prior to substorm onset [*Hubert et al.*, 2006a].

[27] We can also briefly investigate mechanism (1), that is, that the magnetotail is more stable to reconnection when the dayside driving is strong or the ring current is enhanced, or in other words it can exist with more open flux in the tail without reconnection onset. We note in Figures 1g and 1i broad correlation between F_{PC} and SYM-H, that is F_{PC} is larger when SYM-H is more negative. This is especially true on 24 and 31 August during the main phases of the two geomagnetic storms and intensified ring current. To investigate this with a longer time series of polar cap size, we turn to the list of substorm onsets compiled by *Frey et al.* [2004] from the entire duration of the IMAGE mission. For every substorm onset observed by *Frey et al.* [2004] they noted, among other details, the magnetic latitude of the breakup arc. We now use this as a crude proxy for the size of the polar cap at onset: a lower onset latitude indicates a larger polar cap and a greater value of F_{PC}. Figure 8a shows two months (October and November 2001) of onset latitudes from the Frey list, and the corresponding variation in SYM-H. A number of geomagnetic storms are seen in

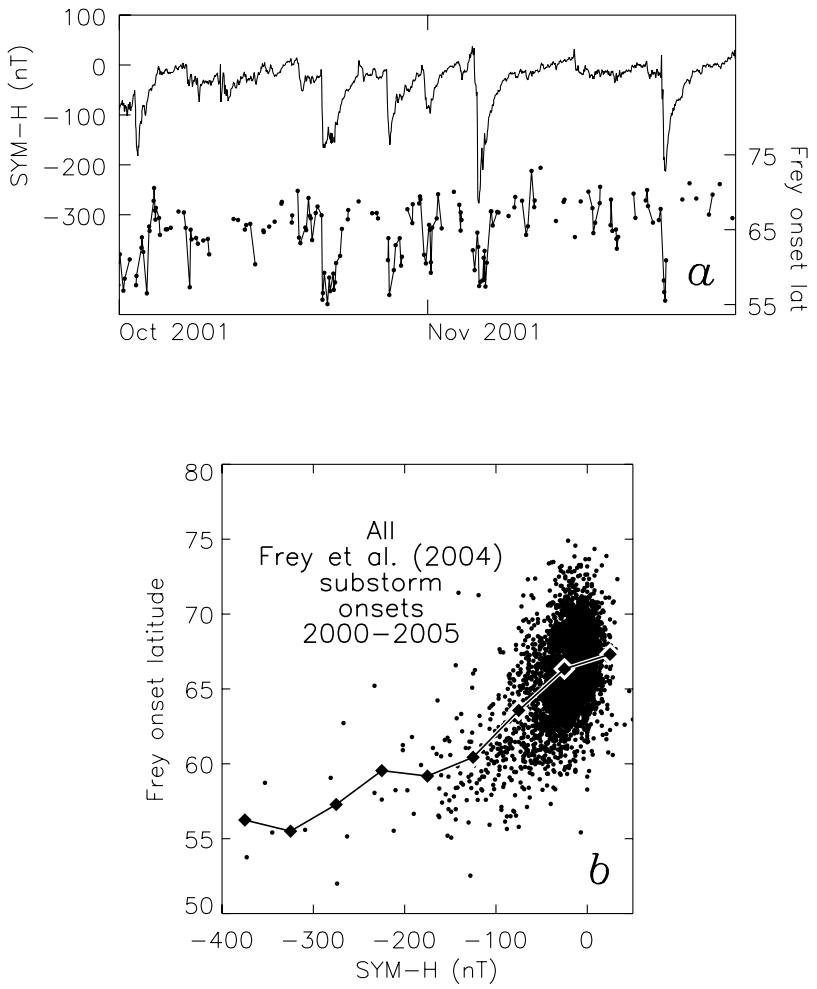

Figure 8. (a) SYM-H for October and November 2001 and the latitude of substorm onsets from the *Frey et al.* [2004] onset list. We use onset latitude as a crude proxy for the open flux in the polar cap at onset, lower latitude indicating enlarged polar cap. (b) Onset latitude as a function of SYM-H for all the *Frey et al.* [2004] onsets, 2000–2005. The diamonds indicate the average onset latitude in 50 nT wide bins.

SYM-H, each of which corresponds to a period during which the substorm onsets are depressed to abnormally low latitudes. In many cases, the variations of the two curves follow very similar patterns. Figure 8b shows all the *Frey et al.* [2004] substorms for the years 2000 to 2005 as a function of SYM-H at the time of onset, indicating a marked decrease in mean onset latitude from 67° for SYM-H $\approx$ 0 nT to 57° for SYM-H ≈ -300 nT. We suggest then that the magnetotail is more stable to reconnection onset in the presence of an enhanced ring current, as previously suggested by *Nakai and Kamide* [2003]. This is possibly due to the enhanced ring current introducing a significant positive B_Z magnetic component into the near-Earth magnetotail, making field lines more dipolar and disfavoring the onset of reconnection until the tail is in a highly stressed state.

4. Conclusions

[28] We have quantified the variation in the open flux in the magnetosphere for an 18 day interval. A 10 day subset of this interval encompasses periods of weak, moderate and strong solar wind driving, the magnetosphere responding with 49 substorms. We find that the occurrence of substorms and the flux closed during individual substorms increases as the driving becomes stronger; each of these increases approximately as the square root of the dayside reconnection rate (Figure 6). We also note that the polar cap becomes larger on average when the solar wind driving is stronger, corresponding to geomagnetic storms. This in part arises as there is a delay between substorm onset and the closure of open flux, and in the meantime open flux is added to the polar cap at the dayside, this additional flux being proportional to the dayside reconnection rate. However, this cannot account for the full increase we observe and suggest that the magnetotail becomes more stable to reconnection when the ring current is enhanced during geomagnetic storms.

Appendix A

[29] *Milan et al.* [2007] showed that the half wave rectified Y component of the motional electric field of the

solar wind, $V_X B_S$ where B_S is the southward component of the IMF, when multiplied by a length scale of $L_M \approx 5\ R_E$, gave a reasonable estimate of the low-latitude dayside reconnection rate Φ_D:

$$\Phi_D = L_M V_X B_S.$$

L_M is interpreted as the effective length scale of the dayside magnetopause reconnection X-line, i.e., the width of the channel in the solar wind that couples to the magnetosphere. This expression can also be written as

$$\Phi_D = \begin{cases} L_M V_X B_{YZ} |\cos\theta|, & |\theta| > 90^o \\ 0 & |\theta| < 90^o \end{cases}$$

where θ is the IMF clock angle and $B_{YZ} = \sqrt{B_Y^2 + B_Z^2}$ is the transverse component of the IMF. One drawback of this relationship is that it predicts that the reconnection rate goes to zero when B_Z is zero or positive, though it is known that low-latitude reconnection can continue when the IMF is directed northward but with a significant B_Y component. Other functional forms have been suggested that represent the clock angle variation of reconnection more realistically, for instance, the *Kan and Lee* [1979] reconnection electric field:

$$E_{KL} = V_X B_{YZ} \sin^2 \frac{1}{2}\theta.$$

We convert this to an overall reconnection voltage by multiplying E_{KL} by an effective length L_{KL}:

$$\Phi_D = L_{KL} E_{KL} = L_{KL} V_X B_{YZ} \sin^2 \frac{1}{2}\theta.$$

Owing to the change in functional form the effective X-line length of 5 R_E is no longer appropriate; we wish to ensure that time-integrated reconnection rates remain of the same order as found by *Milan et al.* [2007], so we use $L_{KL} = \zeta L_M$, where ζ is a normalization factor. This normalization factor would most simply be given by

$$\zeta = \int_{-\pi/2}^{\pi/2} \cos\theta d\theta \Big/ \int_{-\pi}^{\pi} \sin^2 \frac{1}{2}\theta d\theta = \frac{2}{\pi}.$$

However, we must also factor in the frequency distribution of the IMF clock angle, which is found preferentially near 90° and 270°, i.e., the IMF vector lies most often in the equatorial plane; when we do this we find a normalization factor of 0.55, such that $L_{KL} = 2.75 R_E$. Validation of this estimate comes from our demonstration that the mean value of Φ_D matches closely the mean value of the nightside reconnection rate during substorms determined from the observations described in the main body of this paper. It should be noted, however, that the use of our new coupling function or that of *Milan et al.* [2007] does not significantly change out results or interpretation.

[30] **Acknowledgments.** P.D.B. was supported by a PPARC/STFC CASE award, grant PPA/S/C/2006/04488. The ACE data used in this study were accessed through CDAWeb. The authors would like to thank N. F. Ness at the Bartol Research Institute and D. J. McComas of the Southwest Research Institute for use of the MAG and SWEPAM data, respectively. Similarly, we thank E. A. Lucek of Imperial College London for the use of Cluster FGM data. The AU, AL, and SYM-H indices were provided by the Data Analysis Center for Geomagnetism and Space Magnetism, Kyoto University. We would also like to thank H. U. Frey for the use of his substorm onset list.

[31] Amitava Bhattacharjee thanks the reviewers for their assistance in evaluating this paper.

References

Balogh, A., et al. (1997), The Cluster magnetic fields investigation, *Space Sci. Rev.*, *79*, 65–91, doi:10.1023/A:1004970907748.

Balogh, A., et al. (2001), The Cluster Magnetic Field Investigation: Overview of in-flight performance and initial results, *Ann. Geophys.*, *19*, 1207–1217.

Boudouridis, A., E. Zesta, R. Lyons, P. C. Anderson, and D. Lummerzheim (2003), Effect of solar wind pressure pulses on the size and strength of the auroral oval, *J. Geophys. Res.*, *108*(A4), 8012, doi:10.1029/2002JA009373.

Cheng, C. Z. (2004), Physics of substorm growth phase, onset, and dipolarization, *Space Sci. Rev.*, *113*, 207–270, doi:10.1023/B:SPAC.0000042943.59976.0e.

Cowley, S. W. H., and M. Lockwood (1992), Excitation and decay of solar wind-driven flows in the magnetosphere-ionosphere system, *Ann. Geophys.*, *10*, 103–115.

Davis, T. N., and M. Sugiura (1966), Auroral electrojet activity index AE and its universal time variations, *J. Geophys. Res.*, *71*, 785–801.

Dungey, J. W. (1961), Interplanetary magnetic fields and the auroral zones, *Phys. Rev. Lett.*, *6*, 47–48, doi:10.1103/PhysRevLett.6.47.

Dungey, J. W. (1963), The structure of the exosphere or adventures in velocity space, in *Geophysics: The Earth's Environment*, edited by C. De Witt, J. Hieblot, and L. Le Beau, pp. 503–550, Gordon and Breach, New York.

Frey, H. U., S. B. Mende, V. Angelopoulos, and E. F. Donovan (2004), Substorm onset observations by IMAGE-FUV, *J. Geophys. Res.*, *109*, A10304, doi:10.1029/2004JA010607.

Hubert, B., S. E. Milan, A. Grocott, S. W. H. Cowley, and J.-C. Gérard (2006a), Dayside and nightside reconnection rates inferred from IMAGE-FUV and SuperDARN data, *J. Geophys. Res.*, *111*, A03217, doi:10.1029/2005JA011140.

Hubert, B., M. Palmroth, T. V. Laitinen, P. Janhunen, S. E. Milan, A. Grocott, S. W. H. Cowley, T. Pulkkinen, and J.-C. Gérard (2006b), Compression of the Earth's magnetotail by interplanetary shocks directly drives transient magnetic flux closure, *Geophys. Res. Lett.*, *33*, L10105, doi:10.1029/2006GL026008.

Kamide, Y., P. D. Perreault, S.-I. Akasofu, and J. D. Winningham (1977), Dependence of substorm occurrence probability on the interplanetary magnetic field and on the size of the auroral oval, *J. Geophys. Res.*, *82*, 5521–5528, doi:10.1029/JA082i035p05521.

Kan, J. R., and L. C. Lee (1979), Energy coupling function and solar wind-magnetosphere dynamo, *Geophys. Res. Lett.*, *6*, 577–580, doi:10.1029/GL006i007p00577.

Lockwood, M., and S. W. H. Cowley (1992), Ionospheric convection and the substorm cycle, in *Proceedings of the International Conference on Substorms (ICS-1)*, pp. 99–109, Eur. Space Agency, Paris.

McComas, D. J., S. J. Bame, P. Barker, W. C. Feldman, J. L. Phillips, P. Riley, and J. W. Griffee (1998), Solar Wind Electron Proton Alpha Monitor (SWEPAM) for the Advanced Composition Explorer, *Space Sci. Rev.*, *86*, 563–612, doi:10.1023/A:1005040232597.

Mende, S. B., et al. (2000a), Far ultraviolet imaging from the IMAGE spacecraft. 1. System design, *Space Sci. Rev.*, *91*, 243–270, doi:10.1023/A:1005271728567.

Mende, S. B., et al. (2000b), Far ultraviolet imaging from the IMAGE spacecraft. 2. Wideband FUV imaging, *Space Sci. Rev.*, *91*, 271–285, doi:10.1023/A:1005227915363.

Milan, S. E., M. Lester, S. W. H. Cowley, K. Oksavik, M. Brittnacher, R. A. Greenwald, G. Sofko, and J.-P. Villain (2003), Variations in polar cap area during two substorm cycles, *Ann. Geophys.*, *21*, 1121–1140.

Milan, S. E., S. W. H. Cowley, M. Lester, D. M. Wright, J. A. Slavin, M. Fillingim, C. W. Carlson, and H. J. Singer (2004), Response of the magnetotail to changes in open flux content of the magnetosphere, *J. Geophys. Res.*, *109*, A04220, doi:10.1029/2003JA010350.

Milan, S. E., G. Provan, and B. Hubert (2007), Magnetic flux transport in the Dungey cycle: A survey of dayside and nightside reconnection rates, *J. Geophys. Res.*, *112*, A01209, doi:10.1029/2006JA011642.

Nakai, H., and Y. Kamide (2003), Substorm-associated large-scale magnetic field changes in the magnetotail: A prerequisite for "magnetotail deflation" events, *Ann. Geophys.*, *21*, 869–879.

Siscoe, G. L., and T. S. Huang (1985), Polar cap inflation and deflation, *J. Geophys. Res.*, *90*, 543–547, doi:10.1029/JA090iA01p00543.

Slavin, J. A., et al. (2002), Simultaneous observations of earthward flow bursts and plasmoid ejection during magnetospheric substorms, *J. Geophys. Res.*, *107*(A7), 1106, doi:10.1029/2000JA003501.

Smith, C. W., M. H. Acuña, L. F. Burlaga, J. L'Heureux, N. F. Ness, and J. Scheifele (1998), The ACE Magnetic Fields Experiment, *Space Sci. Rev.*, *86*, 613–632, doi:10.1023/A:1005092216668.

Stone, E. C., A. M. Frandsen, R. A. Mewaldt, E. R. Christian, D. Marglies, J. F. Ormes, and F. Snow (1998), The Advanced Composition Explorer, *Space Sci. Rev.*, *86*, 1–22, doi:10.1023/A:1005082526237.

Tanskanen, E. I., J. A. Slavin, D. H. Fairfield, D. G. Sibeck, J. Gjerloev, T. Mukai, A. Ieda, and T. Nagai (2005), Magnetotail response to prolonged southward IMF B_z intervals: Loading, unloading, and continuous magnetospheric dissipation, *J. Geophys. Res.*, *110*, A03216, doi:10.1029/2004JA010561.

Tsyganenko, N. A., and D. P. Stern (1996), Modeling the global magnetic field of the large-scale Birkeland current systems, *J. Geophys. Res.*, *101*, 27,187–27,198, doi:10.1029/96JA02735.

P. D. Boakes and S. E. Milan, Department of Physics and Astronomy, University of Leicester, Leicester LE1 7RH, UK. (steve.milan@ion.le.ac.uk)

B. Hubert, Laboratory of Planetary and Atmospheric Physics, University of Liège, Liège, B-4000 Belgium.